Elsevier Editorial System(tm) for Continental Shelf Research
Manuscript Draft

Manuscript Number: CSR1415R1

Title: Interacting physical, chemical and biological forcing of phytoplankton thin-layer variability in Monterey Bay, California

Article Type: Special Issue; Thin Layers

Keywords: phytoplankton, thin layers, fronts, upwelling ecosystems

Corresponding Author: Dr. John Ryan,

Corresponding Author's Institution: MBARI

First Author: John Ryan

Order of Authors: John Ryan; Margaret A McManus; James M Sullivan

Interacting physical, chemical and biological forcing of phytoplankton thin-layer variability in Monterey Bay, California

John P. Ryan[1], Margaret A. McManus[2], James M. Sullivan[3]

[1]*Monterey Bay Aquarium Research Institute, 7700 Sandholdt Road, Moss Landing, California 95039 USA*
[2]*University of Hawaii at Manoa, Department of Oceanography, 1000 Pope Road, Honolulu, Hawaii 96822 USA*
[3]*University of Rhode Island, Graduate School of Oceanography, South Ferry Road, Narragansett, Rhode Island 02882 USA*

Corresponding author:
John Ryan
Phone: (831) 775-1978
Fax: (831) 775-1620
ryjo@mbari.org

Abstract

During the 2005 *Layered Organization in the Coastal Ocean* (LOCO) field program in Monterey Bay, California, we integrated intensive water column surveys by an autonomous underwater vehicle (AUV) with satellite and mooring data to examine the spatiotemporal scales and processes of phytoplankton thin-layer development. Surveying inner to outer shelf waters repeatedly between August 18 and September 6, the AUV acquired 6,841 profiles. By the criteria: [(1) thickness <= 3 m at the full-width half-maximum, (2) peak chlorophyll at least twice the local background concentrations, and (3) a corresponding peak in optical backscattering], thin layers were detected in 3,978 (58%) of the profiles. Average layer thickness was 1.4 m, and average intensity was 13.5 μg l^{-1} above (3.2 *x*) background. Thin layers were observed at depths between 2.6 and 17.6 m, and their depths showed diurnal vertical migration of the layer phytoplankton populations. Horizontal scales of thin-layer patches ranged from < 100 m to >10,000 m. A thin-layer index (TLI), computed from layer frequency, intensity and thinness, was highest in mid-shelf waters, coincident with a frontal zone between bay waters and an intrusion of low-salinity offshore waters. Satellite observations showed locally enhanced chlorophyll concentrations along the front, and *in situ* observations indicated that phytoplankton may have been affected by locally enhanced nutrient supply in the front and concentration of motile populations in a convergence zone. Minimum TLI was furthest offshore, in the area most affected by the intrusion of offshore, low-chlorophyll waters. Average thin-layer intensity doubled during August 25-29, in parallel with warming at the surface and cooling within and below the thermocline. During this apparent bloom of thin-layer populations, density oscillations in the diurnal frequency band increased by an order of magnitude at the shelfbreak and in near-bottom waters of the inner shelf, indicating the role of internal tidal pumping from Monterey Canyon onto the shelf. This nutrient transport process was mapped by the AUV. Peak

TLI was observed on August 29 during a nighttime survey, when phytoplankton were concentrated in the nutricline. Empirical orthogonal function decomposition of the thin-layer particle size distribution data from this survey showed that throughout the inner to outer shelf survey domain, the layers were dominated by phytoplankton having a cross-section of ~ 50 μm. This is consistent with the size of abundant *Akashiwo sanguinea* cells observed microscopically in water samples. During a subsequent and stronger intrusion of low-salinity offshore waters, spatially-averaged vertical density stratification decreased by > 50%, and phytoplankton thin layers disappeared almost completely from the AUV survey domain.

Keywords: phytoplankton, thin layers, fronts, upwelling ecosystems

1. Introduction

1.1 Environmental Setting

Monterey Bay, California is a dynamic and productive coastal environment in the central California Current System (CCS). Nutrient-rich waters, supporting high primary productivity, shoal by wind-forced coastal upwelling and Ekman pumping, and by internal tidal forcing of transport from Monterey Canyon (Figure 1) onto the shelf (Reid et al., 1958; Barber and Smith, 1981; Shea and Broenkow, 1982; Breaker and Broenkow, 1994; Rosenfeld et al., 1994). Bay waters are a mixture of relatively cold / saline upwelled water and relatively warm / fresh offshore waters of the CCS (Graham and Largier, 1997). The bay environment changes significantly with highly variable influxes of these primary source waters.

The intensity and biological consequences of coastal upwelling in this region are greatest between March and November (Pennington and Chavez, 2000). Within this period, circulation and water mass distributions respond strongly to changes in wind forcing. Equatorward winds produce cold filaments of upwelled waters north and south of the bay, and the upwelling from Point Año Nuevo, 27 km north of the bay, often flows southward across the mouth of the bay (Rosenfeld et al., 1994). A cyclonic gyre forms in the northern bay as a dynamic response to active upwelling (Breaker and Broenkow, 1994). This circulation transports nutrient-rich upwelled waters into the bay and creates a phenomenon known as the 'upwelling shadow', in which residence time and thermal stratification are enhanced (Graham and Largier, 1997). Periods when equatorward winds decrease in intensity (< 3 m s^{-1}) or reverse to poleward are termed 'relaxation events'. During relaxation events, offshore low-salinity waters are transported shoreward (Bolin and Abbott, 1963; Broenkow and Smethie, 1978; Rosenfeld et al., 1994; Ramp et al., 2005). These low salinity waters are warm relative to recently upwelled waters but may be cool relative to bay waters that have warmed during residence in the upwelling shadow.

Responses to relaxation events include rapid flushing of much of the bay by intrusions of offshore low-salinity waters containing relatively low phytoplankton biomass (Ryan et al., 2008a; 2009), as well as mixing and destratification of the inner shelf water column (Storlazzi et al., 2003).

A summary of foundational research on thin layers is presented in the introductory paper of this special issue. Here we summarize some studies of phytoplankton ecology in Monterey Bay relevant to the present study. The upwelling shadow, within which much of the LOCO observations were made, functions as a dinoflagellate "red tide" bloom incubator (Ryan et al., 2005; 2008b; 2009; Rienecker et al., 2008; Kudela et al., 2008). This area has also been observed to host intense and persistent thin layers of toxin-producing diatom species (McManus et al., 2008). Frontal zones formed by inflow of upwelling filaments and offshore waters are important sites for aggregation of diatom and dinoflagellate biomass, as well as phytoplankton thin-layer formation by vertical shear (Pennington and Chavez, 2000; Ryan et al., 2005a; 2008a; 2008b; 2009; Rienecker et al., 2008).

1.2 Research Objectives

The primary objective of this research was to understand the interacting physical, chemical and biological processes that influence phytoplankton thin-layer development in Monterey Bay. Our approach was to (1) intensively map the physical, nutrient and optical properties of inner- to outer-shelf waters (~20 to 200 m depth) at spatial and temporal scales permitting resolution of phytoplankton thin-layer structures, their synoptic patterns of patchiness, and their evolution, and (2) to relate thin-layer variability to regional oceanographic forcing. These intensive AUV observations were also used to quantitatively compare thin-layer attributes observed at the inner shelf array site (Figure 1) with those observed in deeper waters of the bay.

2. Methods

2.1 Dorado autonomous underwater vehicle (AUV) surveys

The MBARI AUV *Dorado* repeatedly occupied a triangular survey track (Figure 1) during the period August 18 to September 6, 2005, taking 6,841 profiles in total. The survey was comprised of two cross-shelf transects and one along-shelf transect, with one of each type of transect extending away from the LOCO primary mooring array site (Figure 1). Of the 20 repeated surveys, 18 were conducted over an 8-day period, between August 25 and September 1, for the purpose of high-resolution thin-layer quantification. The other two surveys, on August 18 and September 6, were for the purpose of thin-layer characterization before and following the intensive AUV observation period.

The AUV was equipped with physical, chemical and optical sensors. We present observations from five sensors: (1) a SeaBird SBE 25 CTD that measured temperature and conductivity, (2) a Paroscientific 8CB/4000-I pressure sensor, (3) a HOBI Labs HS-2 sensor that measured optical backscattering at 470 and 676 nm, centered on a scattering angle of 140°, and chlorophyll fluorescence, (4) an *in situ* ultraviolet spectrophotometer (ISUS) sensor that measured nitrate concentrations (Johnson and Coletti, 2002), and (5) a Sequoia Scientific LISST-100 (Laser In Situ Scattering and Transmissometer) that measured the particle size distribution between 1 and 250 μm. The LISST-100 has proven effective for studying the patchiness and evolution of coastal ocean dinoflagellate and diatom blooms (Rienecker et al., 2008).

At a speed of ~1.5 m s^{-1} and a 30° pitch through yo-yo profiling, the AUV provided synoptic high-resolution sections through shelf waters. A single transit around the 38 km triangular survey track (Figure 1) averaged 342 profiles in ~6.5 hours. Profile depth tracked bottom depth, with the AUV remaining ~4 m above bottom on all profiles. Horizontal resolution thus varied with water depth, ranging from ~15 profiles km^{-1} (70 m $profile^{-1}$) for the along-shelf

transect to ~ 3 profiles km^{-1} (330 m $profile^{-1}$) over Monterey Canyon (Figure 1). Average vertical resolution of optical profile data used to detect thin phytoplankton layers was 0.1 m.

2.2 Quantification of thin-layer attributes

Quantification of thin-layer attributes from the AUV data was consistent with the methods applied to data collected by other researchers using autonomous moored profilers at the main LOCO array site. Specifically, we cross-calibrated AUV fluorometric chlorophyll with that from the moored profiler systems, and we applied the same thin-layer detection and quantification methods (Sullivan et al., this issue). The criteria used for thin layers were: (1) intensity of the chlorophyll layer peak must be at least twice the local background chlorophyll concentration; (2) the fluorometric chlorophyll peak must coincide with a local peak in optical backscattering, to ensure that the fluorescence profile structure is also a biomass maximum and not due to inhibition of chlorophyll fluorescence at high light intensities near the surface (Cullen and Eppley, 1981; Holm-Hansen et al., 2000); (3) layer thickness at the full-width half-max (FWHM) must be <= 3 m. Dekshenieks et al. (2001) established an upper limit of 5 m in their definition of a thin layer, because it was less than the 5-m scales routinely sampled with bottles and nets. The work published in Dekshenieks et al. (2001) was undertaken in 1996; this was the first study to put forward criterion to define thin-layer structures. After more than a decade of additional research on thin layers, we now use a 3-m cutoff because the statistics of multiple studies support this criterion. In their analysis of thin layers in East Sound, WA, Dekshenieks et al. (2001) found that layers ranged in thickness from 0.12 to 3.61 m, with 80% < 2 m. In a later study in Monterey Bay CA, McManus et al. (2008) tracked a thin layer, measuring between 0.1 and 3.0 m thick (85%< 2 m), for 7 days near the base of the pycnocline. Analysis of 3 years of moored profiler data from Monterey Bay showed that vast majority of layers were <= 3 m thick (Sullivan, et al., this issue). A recent publication describing thin layers detected with LIDAR in

diverse marine environments also determined that 3 m was an appropriate criterion for defining thin layers in many environments (Churnside & Donaghay, 2009).

Layer intensity was quantified as the magnitude of the chlorophyll peak above the local background, using a linear baseline method (Sullivan et al., this issue). Here we term this intensity measurement: chlorophyll line height (CLH). Once the AUV data set was reduced to statistics of the time, location $\{x,y,z\}$, thickness and intensity of layers, further statistical characterizations were computed. To examine spatial patterns, average layer attributes were computed within along-track spatial bins. Bin boundaries were defined from 10 evenly spaced latitude bands within the 16.3 km north-south extent of the survey (Figure 1). To examine temporal patterns, average layer attributes were computed for each survey. From spatially and temporally binned statistics, a multi-parameter thin-layer index (TLI) was computed as the product of frequency, intensity and thinness. TLI was normalized between the minimum and maximum and is presented as a relative index ranging between 0 and 1. To quantify horizontal scales, thin-layer patches were defined as clusters of adjacent profiles in which thin layers were consistently detected. The horizontal scales of the 440 detected patches were computed from the along-track distance spanned by each cluster of thin-layer profiles. Determination of patch continuity was constrained by the horizontal resolution of profiles, which varied with water depth between ~15 and 3 profiles km^{-1} (Section 2.1).

To characterize the phytoplankton populations in the thin layers, we analyzed the particle size distribution (PSD) data from the LISST-100 (Section 2.1) using empirical orthogonal function (EOF) decomposition. For the survey having the highest TLI, we present EOF results for PSD data in the size range 1-100 μm.

2.3 Moorings

To describe oceanographic variability we used hourly measurements from two long-term

MBARI moorings, M0 in northern shelf waters within the AUV survey domain and M1 in the central bay mouth, as well as hourly profiles from station S (Figure 1). Sensors of M0 and M1 are described in Ryan et al. (2009); the moored profiler system is described by Sullivan et al. (this issue). To illustrate water mass changes in the AUV survey domain, average temperature and salinity were computed from sensors at 3.5, 10 and 20 m at M0. To quantify temporal variation of internal tidal forcing, we analyzed density time series at two locations: (1) at 150 m at M1, and (2) below 15 m at station S (Figure 1). The hourly density time series were constrained to the limiting duration of station S profiler data. Using the methods and software of Torrence and Compo (1998), the wavelet power spectrum was computed for each time series, and the scale-averaged wavelet power for the diurnal band (0.8 to 1.2 days) was calculated.

2.4 MODIS satellite data

To examine synoptic patterns relevant to water mass and phytoplankton distributions, we used MODIS (Moderate Resolution Imaging Spectroradiometer) satellite data. Details of MODIS processing are in Ryan et al. (2009).

3. Results and Discussion

3.1 Regional variability

Between mid-August and early September 2005 at M0, the dominant variation in water properties was alternation of relatively warm / saline waters and relatively cool / fresh waters (Figure 2). This pattern is distinct from the bay's source water mass properties of cool / saline upwelled waters and warm / fresh offshore CCS waters, indicating the role of local physical processes in modifying source waters. Large decreases in salinity occurred rapidly, consistent with passage of fronts, beginning on August 24 and September 3 and 5. The AUV surveys showed that these rapid changes were caused by intrusions of low-salinity offshore waters into

the study domain (Figure 3). By August 25, the first low-salinity intrusion occupied the southern region of the AUV survey domain (Figure 3b). The intrusion submerged beneath warm surface waters while spreading northward ~ 15 km (Figure 3b-f) and by August 29 reached the furthest inner-shelf waters surveyed, and the LOCO array (Figure 3f).

Satellite imagery from August 25 showed patterns related to the early stages of the intrusion. Blue, low-chlorophyll waters occupied the southern bay, while green-brown, high-chlorophyll waters occupied the northern bay (Figure 4a,b). The low-chlorophyll waters corresponded with intrusion of offshore, low-salinity waters (Figure 3b). The frontal boundary, oriented northwest \ southeast, exhibited patchy, locally enhanced color and chlorophyll (Figure 4a,b). The highest chlorophyll concentrations and strongest water coloration were in nearshore waters, inshore of the LOCO array and the AUV survey track (Figure 4a,b). Within the frontal zone between the intruding offshore waters and resident bay waters was the coolest SST (Figure 4c). The cool SST was not due to advection of an upwelling filament into the bay, which would have coincided with high-salinity anomalies outcropping to the surface rather than the observed low-salinity anomaly (Figures 2, 3). Vertical circulation and mixing in the front probably caused the cool SST. The coldest subsurface waters reached the shallowest depth in the frontal zone, where the salinity distributions indicated horizontal interleaving (white + signs in Figure 3b,c). Also, the deepest penetration of low salinity waters occurred along the leading (northward flowing) edge of the intrusion. These vertical displacements indicate enhanced vertical circulation in the front. Thus, the high chlorophyll concentrations in the frontal zone (Figure 4) may have resulted, in part, from growth enhancement via local nutrient supply.

3.2 Thin-layer statistics

Of the 6,841 AUV profiles, 58% (n=3,978) contained phytoplankton layer structures that met all thin-layer criteria. This percentage is close to that found from moored profiling time-

series at the array site (56%; Sullivan et al., this issue). The depths of thin-layer peaks ranged between 2.6 and 17.6 m. The overall mean thin-layer intensity was 13.5 $\mu g\ l^{-1}$ above background (3.2 *x* background), and mean thickness was 1.4 m. Cumulative frequency distributions (Figure 5) show that layer vertical scale (thickness) was the most evenly distributed layer attribute, while layer horizontal scale had the most skewed distribution. The horizontal scales of the 440 thin-layer patches ranged from < 100 m to > 10,000 m; the median patch size was 320 m. The largest patch, exceeding 10 km, was mapped along the most offshore transect (Figure 1) on August 27. Median layer statistics are close to those quantified from moored profiling time-series at the LOCO array site (Sullivan et al., this issue). Median thickness was exactly the same (1.3 m). Intensity was slightly higher for the AUV data set (2.8x versus 2.5x), consistent with the finding of higher average layer intensity seaward of the array (Section 3.3).

3.3 Spatial variation in thin layers and related processes

Average layer attributes exhibited significant spatial heterogeneity (Figure 6). The frequency of thin-layer detection (Figure 6a) ranged from 27% to 81%, with more frequent presence seaward of the shallow-water LOCO array, and the maximum between the 50 and 75 m isobaths. The lowest frequencies were at the southern limit of the survey, over Monterey Canyon (Figure 1), the location that would have been most affected by the low-salinity, low-chlorophyll intrusion (Figures 3, 4). Average layer intensity ranged between 9.1 and 14.9 $\mu g\ l^{-1}$ above background (Figure 6b). The highest average intensities were observed in two areas of the inner shelf (< 25 m depth, west and southeast of the array), and in mid-shelf waters (south of the array between the 50 and 75 m isobaths). Average layer thickness (Figure 6c) ranged between 1.2 and 1.6 m. In general, layers were thinner in deeper waters, and specifically they were thinnest in mid-shelf waters, between the 50 and 75 m isobath. The multi-parameter TLI showed that overall, thin layers were most frequent, intense and thin in the mid-shelf waters between the 50

and 75 m isobaths (Figure 6d; TLI is normalized to a relative scale between 0 and 1). This same zone also exhibited the maximum salinity variance in the upper 20 m (Figure 6e). This high salinity variance was caused by the influx of a low-salinity intrusion and mixing of water masses in a frontal zone (Figure 3; Section 3.1). Enhanced layer thinness in the frontal zone is consistent with influence of enhanced vertical shear, which can be locally intensified in frontal currents (Franks, 1995; Dekshenieks et al., 2001; Ryan et al., 2008a). The enhanced layer intensity in the front may have developed from local nutrient enrichment (Section 3.1), as well as aggregation of biomass in what was probably a convergence zone (Figures 3, 4). Phytoplankton motility is required for aggregation in a convergent front, and it was observed (Section 3.4).

3.4 Vertical migration of a dominant phytoplankton size-class

The average depth of the thin layers exhibited diurnal variation (Figure 7). Layers were on average about twice as deep and in waters 1°C colder during the night as they were during the day. The populations were nearest the surface between ~ 10 am and 2 pm and deepest at ~ 2 am. This characterization of diurnal vertical migration throughout the AUV survey domain is consistent with the description of this process at the LOCO array site for the dinoflagellate that dominated the phytoplankton assemblage during this period, *Akashiwo sanguinea* (Sullivan et al., this issue), as well as earlier lab and field studies of this species (previously identified as *Gymnodinium sanguineum* or *splendens*; Kiefer and Lasker, 1975; Cullen and Horrigan, 1981). Downward migration was clearly responsive to nutrient levels. Data from a nighttime survey (Figure 8) shows the layers aligned with a nitrate isopleth that diverged significantly from isotherms. The subsurface nitrate minimum (Figure 8b) had no corresponding structure in the salinity field (not shown), suggesting that nutrient uptake patterns by the vertically migrating populations may have created the nutrient minimum, as described for a *Gymnodinium catenatum* bloom in Ría de Vigo, Spain (Fraga et al., 1992).

Water samples from the array showed the prevalence of *Akashiwo sanguinea* in the NE bay (Rines et al., this issue; Sullivan et al., this issue). Measurements of the particle size distribution (PSD) indicate that this prevalence extended throughout the greater northern shelf. The average cross-sectional dimension of *A. sanguinea* cells measured microscopically was ~ 50 μm (Rines et al., this issue). Laboratory and field tests have shown that for populations of dinoflagellates whose cells are pseudo-spherical, the LISST-100 instrument produces a single peak at the average cell cross-sectional dimension (Rienecker et al., 2008). At the peak of average thin-layer intensity (survey shown in Figure 8; temporal variation examined in section 3.5), the PSD within thin layers was dominated by cells having a cross-sectional scale consistent with that of *A. sanguinea*. The first EOF of the thin-layer PSD data, accounting for 97% of the variance, exhibited a peak at 50 μm (Figure 9). This PSD dominance was prevalent throughout the intensive AUV time-series of August 25 - September 1.

3.5 Temporal variation in thin layers and related processes

Thin-layer attributes averaged for each of the 20 laps around the triangular survey (Figure 1) exhibited patterns related to the changing environmental conditions. Thin-layer encounter frequencies were low during the preliminary survey on August 18 and the final survey on September 6 (Figure 10a). During the intensive AUV survey period, August 25 - September 1, thin-layer encounter frequency was mostly > 50%. Average layer thickness was < 2 m for all surveys, except for the final survey on September 6 when frequency was also at a minimum (1%). Average layer intensity rose to a maximum between August 25 and 29, ranging from ~7.1 to 19.4 μg l^{-1} above background (Figure 10b). The multi-parameter TLI peaked on August 29, when intensity was at its peak, thickness was near the minimum, and frequency was near the maximum (open symbols in Figure 10a,b). In examining these changes, it is important to evaluate the possibility of time-of-day affecting thin-layer detection and quantification, which

would be important for vertically migrating populations. The times of the AUV surveys are shown in Figures 2 and 10. For the period of thin-layer intensification between August 25 and 29, an AUV survey began within 2 hours of sunset each day, and at least one survey began in early to mid-afternoon each day. Therefore, we conclude that the increase in thin-layer intensity during August 25-29 was a biological event and not an artifact of variability in daily sampling periods.

The approximate doubling of thin-layer intensity coincided with a ~50% increase of average chlorophyll concentrations in the upper 20 m (Figure 10c). Increases in thin-layer intensity were evident at all spatial bins (bin locations shown in Figure 6) except for the southernmost area seaward of the frontal zone (Figure 4). These results suggest a northern shelf bloom dominated by thin-layer forming phytoplankton. The biological trends corresponded closely with physical trends. During the rise in average chlorophyll and thin-layer intensity, vertical density stratification between 3 and 15 m depth increased by 44% (Figure 10d). This stratification change was caused primarily by near-surface warming and simultaneous cooling at 15 m (Figures 10d; 3b-f). Salinity at these depths showed opposite trends, with decreasing salinity at 3 m and increasing salinity at 15 m (not shown). Enhancement of stratification while surface nutrient concentrations were low (Figure 8b) would favor dinoflagellates that can migrate vertically (Figure 7) to acquire nutrients in the nutricline. Also during August 26-30, daily integrated photosynthetically active radiation was at a maximum of the AUV operations period (measured at M1; not shown), thus supporting greater capacity for photosynthesis.

As suggested by the thermocline cooling, enhanced nutrient availability in the thermocline may have supported growth of vertically-migrating phytoplankton. We did not measure nutrient uptake by phytoplankton or its variability. Here we utilize oceanographic observations to evaluate potential nutrient supply mechanisms. As described in Section 3.1,

mooring and AUV data indicate that no upwelling filaments were advected into the study domain. Although vertical circulation in the front was evidently an important local nutrient supply mechanism, thin-layer intensity increased throughout the AUV survey domain during August 25-29. Animation of the AUV volume time-series (as in Figure 3) indicated that cold, nutrient-rich waters were transported from Monterey Canyon onto the shelf, all the way to the array site in the NE bay. These patterns were consistent with a known mechanism of nutrient flux forced by internal tidal fluctuations (Shea and Broenkow, 1982). During the period of overlapping moored observations at M1 and station S (Figure 1), internal tidal oscillations at M1, 150 m depth (the depth of the shelfbreak) were dominated by the diurnal frequency band (Figure 11a). The intensity of diurnal oscillations increased by a factor of 16 between August 24 and 29, and concurrently by a factor of 8 at station S (Figure 11b). These time-series thus indicate intensification of internal tidal forcing that can supply nutrients to the shelf ecosystem. Boluses of cold, saline water on the shelf, as described by Shea and Broenkow (1982), are evident in the synoptic maps (Figure 3), and a high-resolution time-series of the nitrate field illustrates the transport process (Figure 12). This pattern was observed through multiple tidal cycles, including a series of sections along the offshore AUV transect (Figure 12 shows the inshore legs). Although observed along vertical sections in previous studies (Shea and Broenkow, 1982), this study (Figure 12), and subsequent studies (Ryan, unpubl. data), the spatial scales of this mechanism of nutrient supply, as well as its dependencies upon regional wind forcing, lower frequency tidal forcing, subtidal circulation, and mesoscale dynamics, have not been adequately quantified. More thorough observations and numerical simulations are required to better understand the consequences of this nutrient supply mechanism for the bay ecosystem.

Minimum TLI was observed in the September 6 survey (Figure 10b), following the second and stronger intrusion of low salinity waters (Figures 2, 3g). Like the previous intrusion,

this event was accompanied by cooling. In addition to plankton community changes that would have accompanied water mass intrusion, shallow density stratification (as in Figure 10d) decreased by more than 50% between September 1 and 6 (cf. Figure 3f,g). This weakening of stratification would have affected the biological-physical interactions that had favored vertically migratory dinoflagellates.

3.6 Implications for harmful algal bloom (HAB) ecology

The 2005 LOCO array site was located in shallow waters of the northern Monterey Bay upwelling shadow, a region known to incubate, spread and retain dinoflagellate blooms (Ryan et al., 2005; 2008b; 2009; Rienecker et al., 2008; Kudela et al., 2008). Some of the dinoflagellates found in this region of Monterey Bay, including *Alexandrium catanella* and *Dinophysis sp.* (Ryan et al., 2008b), can cause harm through production of toxins. *Cochlodinium cf fulvescens*, which has been a significant bloom former in this region since 2004 (Curtiss et al., 2008; Kudela et al., 2008), can cause fish and shellfish mortality events. *Akashiwo sanguinea*, the dinoflagellate that dominated thin-layer variability during the 2005 LOCO study, has been recently linked to a previously unknown harmful effect. External coating of seabirds by organic matter from an *Akashiwo* bloom in Monterey Bay impaired the insulating function of feathers, causing bird morbidity and mortality by hypothermia (Jessup et al., 2009). The LOCO 2005 study connects thin-layer ecology of vertically migratory dinoflagellates to understanding HABs that develop from dinoflagellate populations, which are favored by the stratified environment of the Monterey Bay upwelling shadow. Linkages between thin layers and harmful diatom species have also been examined for this region of Monterey Bay. Intense concentration of toxin-producing *Pseudo-nitzschia* populations in subsurface thin layers has been observed in this region and hypothesized as a mechanism for 'cryptic' HABs (McManus et al., 2008).

HAB dynamics and impacts are influenced by biological-physical interactions occurring

at multiple scales, and these interactions may be an essential part of the life-history strategies of HAB species (Donaghay and Osborn, 1997). Achieving high spatial and temporal resolution of variability in thin layers and their environment, the present study detected interactions at multiple scales. On vertical scales <10 m, we observed vertical migration and clear association of migratory populations with the nutricline, which diverged significantly from the thermocline in the upwelling shadow. On scales of a few kilometers in the horizontal, we observed concentration of phytoplankton biomass in a frontal zone, evident in satellite remote sensing images and *in situ* thin-layer intensity. Physical influences on nutrient supply (frontal interleaving) and biomass aggregation (convergence) were implicated. On scales > 10 kilometers, we observed multiple biological-physical interactions. Water mass intrusions from offshore impacted the entire study domain. While thin layers intensified during an intrusion that submerged beneath the thermocline, thin layers disappeared during a subsequent intrusion exhibiting stronger flushing of the upper water column and accompanying breakdown of stratification. As studies with remote sensing and drifters have shown, flushing events resulting from variability in wind forcing can rapidly transport blooms that are incubated in the upwelling shadow to coastal waters north and south of Monterey Bay (Woodson et al., 2009). The dinoflagellate species that tend to form the most intense blooms in Monterey Bay are characterized by a life-history strategy that is well adapted to the dynamic changes typical of coastal upwelling systems (Smayda, 2002; Kudela et al., 2008). Also at scales > 10 km, we observed internal tidal pumping of nutrients onto the shelf up to the thermocline, in a way that would be favorable to dinoflagellates. The relative influence of canyon upwelling that can allow stratification to persist or intensify, versus influx of destratified upwelling filaments, represents a primary modulation for the competitive interactions of diatoms and dinoflagellates in this environment.

Conclusions

The application of high-resolution vertical profiling in aquatic ecology during recent decades has yielded important insights into the processes, complexities and consequences of fine-scale ecosystem structure. The platforms, sensors, and techniques have evolved significantly from early ship-based profiling that began to reveal fine-scale biological structure (e.g. Derenbach et al., 1979). Optical and acoustic sensor developments have contributed greatly to biological layer detection and quantification. Platform developments, such as autonomous vehicles and autonomous profilers deployed from ships and on moorings, have supported multidisciplinary measurements at the scales required to understand ecosystem structure and processes. Beyond the advancements of *in situ* measurement technologies focused upon fine-scale ecology, advancement of this research field requires effective integration with ocean observing systems that provide regional in situ and remote sensing data, and coupled physical-chemical-biological models that can accurately quantify ecosystem processes.

Acknowledgments

This research was supported by ONR grant N00014-04-1-0311 and by the David and Lucile Packard Foundation. We thank MBARI AUV operations personnel H. Thomas, D. Conlin and D. Thompson, and R/V Zephyr and R/V Robert Gordon Sproul personnel who supported AUV operations. M0 and M1 mooring support and data processing were provided by MBARI, with funding for M0 support through the Center for Integrated Marine Technology (NOAA NA160C2936). MODIS data were provided by the Level 1 and Atmosphere Archive and Distribution System (LAADS), and MODIS data processing utilized software developed by the NASA SeaDAS and MODIS Ocean Biology Processing Groups.

References

Barber R.T., Smith, R.L., 1981. Coastal upwelling ecosystems, p. 31-68. In Longhurst, A.R. (Ed.), Analysis of Marine Ecosystems, Academic.

Bolin, R.L., Abbott, D.P., 1963. Studies on the marine climate and phytoplankton of the central coastal area of California, 1954-1960. California Cooperative Oceanic Fisheries Investigations 9:23-45.

Breaker, L.C., Broenkow, W.W., 1994. The circulation of Monterey Bay and related processes. Oceanography and Marine Biology: An Annual Review 32:1-64.

Broenkow, W.W., Smethie, W.M., 1978. Surface circulation and replacement of water in Monterey Bay. Estuarine and Coastal Marine Science 6:583-603.

Churnside, J.H., Donaghay, P.L., 2009. Thin scattering layers observed by airborne lidar. ICES Journal of Marine Science, 66, doi:10.1093/icesjms/fsp029.

Cullen, J. J., Eppley, R.W., 1981. Chlorophyll maximum layers of the Southern California Bight and possible mechanisms of their formation and maintenance. Oceanol. Acta 4: 23-32.

Cullen, J. J., Horrigan, S. G., 1981. Effects of nitrate on the diurnal vertical migration, carbon to nitrogen ratio, and the photosynthetic capacity of the dinoflagellate, *Gymnodinium splendens*. Mar. Biol. 62: 81-89.

Curtiss, C.C., Langlois, G.W., Busse, L.B., Mazzillo, F., Silver, M.W., 2008. The emergence of *Cochlodinium* along the California Coast (USA). Harmful Algae 7:337-346.

Dekshenieks M.M., Donaghay, P.L., Sullivan J.M., Rines J.E.B., Osborn T.R., Twardowski M.S. (2001) Temporal and spatial occurrence of thin phytoplankton layers in relation to physical processes. Mar Ecol Prog Ser 223:61–71.

Donaghay, P.L., Osborn, T. R., 1997. Toward a theory of biological-physical control of harmful algal bloom dynamics and impacts. Limnol. Oceanogr. 42:1283-1296.

Fraga, F., Pérez, F.F., Figueiras, F.G., Ríos, A.F., 1992. Stoichiometric variations of N,P,C and O_2 during a *Gymnodinium catenatum* red tide and their interpretation. Marine Ecology Progress Series 87: 123-134.

Graham, W.M., Largier J.L., 1997. Upwelling shadows as nearshore retention sites: the example of northern Monterey Bay. Continental Shelf Research 17, 509-532.

Franks, PJS, 1995. Thin layers of phytoplankton: a model of formation by near-inertial wave shear. Deep-Sea Res Part I 42:75–91phys Res 110:C07013

Holm-Hansen, O., Amos, A. F., Hewes, C. D., 2000. Reliability of estimating chlorophyll a concentrations in Antarctic waters by measurement of in situ chlorophyll a fluorescence. Marine Ecology Progress Series 196: 103-110.

Jessup, D.A., Miller, M.A., Ryan, J.P., Nevins, H.M., Kerkering, H.A., Mekebri, A. Crand, D.B., Johnson, T.A., Kudela, R.M., 2009. Mass stranding of marine birds caused by a surfactant-producing red tide. PLOS ONE 4(2): e4550. doi:10.1371/journal.pone.0004550.

Johnson, K.S., Coletti, L.J., 2002. In situ ultraviolet spectrophotometry for high resolution and long term monitoring of nitrate, bromide and bisulfide in the ocean. Deep-Sea Research I 49: 1291-1305.

Kiefer, D.A., Lasker, R., 1975. Two blooms of *Gymnodinium splendens*, an unarmoured dinoflagellate. Fisheries Bulletin 73: 675-678.

Kudela, R.M., Ryan, J.P., Blakely, M.D., Lane, J.Q., Peterson, T.D., 2008. Linking the physiology and ecology of *Cochlodinium* to better understand harmful algal bloom events: a comparative approach. Harmful Algae, 7: 278-292.

McManus, M.A., Kudela, R.M., Silver, M.W., Steward, G.F., Donaghay, P.L., Sullivan, J.M., 2008. Cryptic Blooms: Are Thin Layers the Missing Connection? Estuaries and Coasts: J CERF DOI 10.1007/s12237-007-9025-4.

Pennington J.T., Chavez, F.P., 2000. Seasonal fluctuations of temperature, salinity, nitrate, chlorophyll and primary production at station H3/M1 over 1989-1996 in Monterey Bay, California. Deep-Sea Research II 47, 947-973.

Ramp, S.R., Paduan, J.D., Shulman, I., Kindle, J., Bahr, F.L., and Chavez, F.P., 2005. Observations of upwelling and relaxation events in the northern Monterey Bay during August 2000. J. Geophys. Res. 110, C07013, doi:10.1029/2004JC002538.

Reid, J.L., Roden, G.I., Wyllie, J.G., 1958. Studies of the California Current System. California Cooperative Oceanic Fisheries Investigations, Progress Report, 1 July 1956 – 1 January 1958, pp. 27-56.

Rienecker, E.R., Ryan, J.P., Marin III, R., Blum, M., Dietz, C., Chavez, F.P., 2008. Synoptic mapping of the phytoplankton size distribution, with applications to the ecology of red tides and harmful algal blooms, Limnology and Oceanography: Methods 6, 153-161.

Rines, J., et al., Fine scale temporal and spatial variability in phytoplankton composition in Monterey Bay, CA., this issue.

Rosenfeld, L.K., Schwing, F.B., Garfield, N., Tracy, D.E., 1994. Bifurcated flow from an upwelling center: a cold water source for Monterey Bay. Continental Shelf Research 14:931-964.

Ryan, J.P., Dierssen, H.M., Kudela, R.M., Scholin, C.A., Johnson, K.S., Sullivan, J.M., Fischer, A.M., Rienecker, E.V., McEnaney, P.R., Chavez, F.P., 2005a. Coastal ocean physics and red tides: an example from Monterey Bay, California. Oceanography 18, 246-255.

Ryan, J.P., McManus, M.A., Paduan, J.D., Chavez, F.P., 2008a. Phytoplankton thin layers in Monterey Bay, California. Marine Ecology Progress Series, 354, 21-34.

Ryan, J.P., Gower, J.F.R., King, S.A., Bissett, W.P., Fischer, A.M., Kudela, R.M., Kolber, Z., Mazzillo, F., Rienecker, E.R., Chavez, F.P., 2008b. A coastal ocean extreme bloom

incubator. Geophysical Research Letters, 35, L12602, doi:10.1029/2008GL034081.

Ryan, J.P., Fischer, A.M., Kudela, R.M., Gower, J.F.R., King, S.A., Marin, R. III, Chavez, F.P., 2009. Influences of upwelling and downwelling winds on red tide bloom dynamics in Monterey Bay, California. Continental Shelf Research, 29: 785–795.

Shea R.E., Broenkow W.W., 1982. The role of internal tides in the nutrient enrichment of Monterey Bay, California. Estuar Coast Shelf Sci 15:57–66.

Smayda, T., 2002. Adaptive ecology, growth strategies, and the global bloom expansion of dinoflagellates. J. Oceanogr. 58, 281–291.

Storlazzi, C.D., McManus, M,.A., Figurski, J.D., 2003. Long-term, high-frequency current and temperature measurements along central California: insights into upwelling/relaxation and internal waves on the inner shelf. Continental Shelf Research 23: 901-918.

Sullivan, J.S., et al. Coastal thin layer dynamics: consequences to biology and optics, this issue.

Torrence, C., Compo, G. P., 1998. A practical guide to wavelet analysis. Bull. Am. Met. Soc. 79:61-78.

Woodson, C.B., Washburn A.L., Barth, J.A., Hoover, D.J., Kirincich, A.R., McManus, M.A., Ryan, J.P., Tyburczy, J., 2009. The northern Monterey Bay upwelling shadow front: Observations of a coastally- and surface-trapped buoyant plume. J. Geophys. Res., submitted.

Figure Captions

Figure 1. Map of the study region, Monterey Bay, California. The triangular track over the northern shelf in the bay shows the AUV survey path that was repeatedly occupied. The AUV track is 38 km along-track and spans 16.3 km north-south; 7 km east-west. Data from the M0 (70 m water depth) and M1 (1000 m water depth) moorings provided oceanographic data. The 3 black circles in the northeastern bay show the locations of the LOCO primary mooring sites, data from station S are used in this study.

Figure 2. Variability at M0 during LOCO 2005; time is GMT. Salinity and temperature are averages for the upper 20 m. Bars along the top indicate periods when the AUV was surveying along the track shown in Figure 1; bar length indicates 1, 2 or 3 consecutive laps of the AUV track in a single, continuous survey. Bars along the bottom identify the laps for which density, salinity and temperature are shown in Figure 3.

Figure 3. Water mass and frontal variability. High-resolution volume maps are from the times indicated by the bars along the bottom of Figure 2. The depth range shown is 2 to 60 m, the view is from the south, and the location of mooring M0 is shown (Figure 1). White + symbols in (b) and (c) indicate features described in the text (Section 3.1).

Figure 4. Moderate Resolution Imaging Spectroradiometer (MODIS) satellite imagery showing water mass distributions and frontal patterns. Image data are from August 25, 2005, when intrusion of low-salinity offshore waters into Monterey Bay was in progress (Figure 3b). Mooring and AUV survey locations, as in Figure 1, are shown. The vectors at moorings M1 and M0 represents the shallowest measured average velocity during August 23-25, 10 m at M0 and 20 m at M1.

Figure 5. Cumulative frequency distributions of thin-layer attributes for the full AUV data set, computed from 3,978 thin-layer profiles (Section 2.2). CLH is chlorophyll line height, a

measure of layer intensity above the local background. The median for each parameter is marked by a diamond on the x-axis.

Figure 6. Average spatially binned thin-layer attributes, computed from 6,841 AUV profiles, 3,978 of which contained thin-layer structures, from 20 repeated surveys along the track shown in Figure 1. Isobaths are shown in gray in all panels; isobath depths (m) are noted in (a). Frequency is the percent of profiles containing phytoplankton thin-layer structures. CLH is chlorophyll line height, a measure of layer intensity above the local background, and TLI is a normalized (0-1 scale) multi-parameter thin-layer index (Section 2.2). V(S) is the variance in salinity within the upper 20 m.

Figure 7. Diurnal variability in average thin-layer depth and temperature within 4-hour windows, computed from all 3,978 thin-layer profiles. Bars show ±1 standard deviation.

Figure 8. Chlorophyll, nitrate and temperature along the AUV survey track, from a nighttime survey that began at (local time) 8:05 pm (after sunset) on August 28 and finished at 2:35 am on August 29. The white contour in all panels is the same reference nitrate isopleth (3 μM).

Figure 9. First empirical orthogonal function (Section 2.2) of the particle size distribution for all phytoplankton thin layers detected in the survey shown in Figure 8. The concentration peak represents the maximum concentration detected in all thin-layer profiles from this survey.

Figure 10. Temporal variability in thin-layer attributes relative to environmental conditions. Each point represents an average for a single iteration of the track shown in Figure 1; time is GMT. (a) layer frequency (percent of profiles having thin-layer structures) and thickness; (b) layer intensity (CLH) and the normalized multi-parameter thin-layer index (TLI) (Section 2.2). Open symbols in (a) and (b) indicate the survey having the maximum TLI; bio-optical, nutrient and physical conditions during this TLI peak survey are shown in Figure 8. (c) Thin-layer CLH and average chlorophyll concentrations in the depth range 2-20 m; (d) temperature at 3 and 15 m

depth, and the density difference between 15 and 3 m depth. Time series in (c) and (d) were smoothed with a 3-point running mean.

Figure 11. Intensification of internal tidal forcing coincident with thin-layer intensification. (a) average wavelet power as a function of period, computed from density at 150 m at M1. The time-series analysis was constrained to the shorter period of the concurrent station S profiling. (b) Wavelet power in the diurnal frequency band (0.8 to 1.2 day period) from density time series at 150 m at M1 and below 15 m at station S (locations in Figure 1). For intercomparison, results for each site were normalized between their minimum and maximum values; the maximum power for M1 (S) is a factor of 16 (8) times greater than the minimum.

Figure 12. Illustration of northward nutrient flux below the thermocline caused by internal tidal pumping from Monterey Canyon. The vertical sections of nitrate were consecutively mapped on August 28-29. The segment of the full AUV survey shown is indicated in the upper-left inset. The black contour in all panels (13 μM) highlights the northward movement of high nitrate waters below the thermocline. The inset in (a) shows bottom pressure from an ADCP on the shelf, illustrating the tidal oscillations (gray line) and the start of the consecutive AUV surveys (black circles).

Figure 1

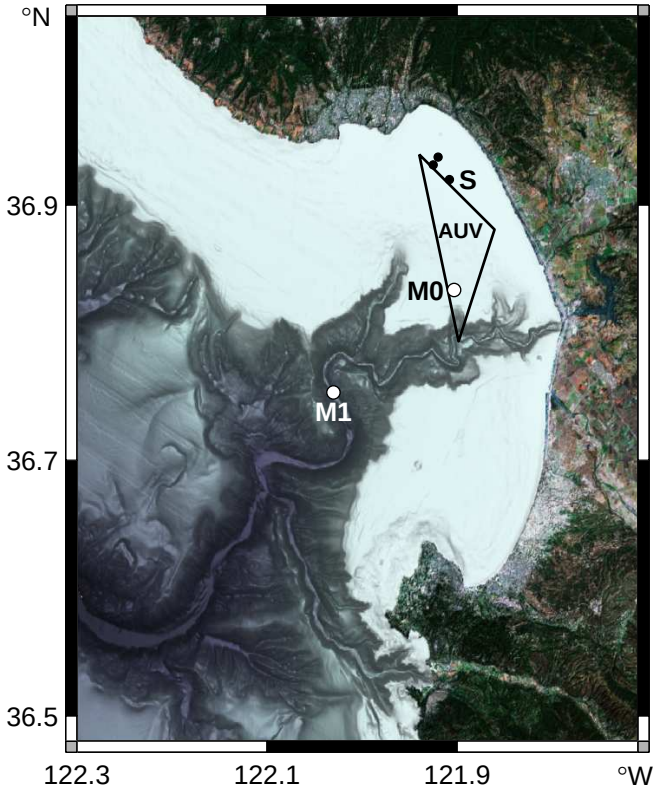

Figure 2

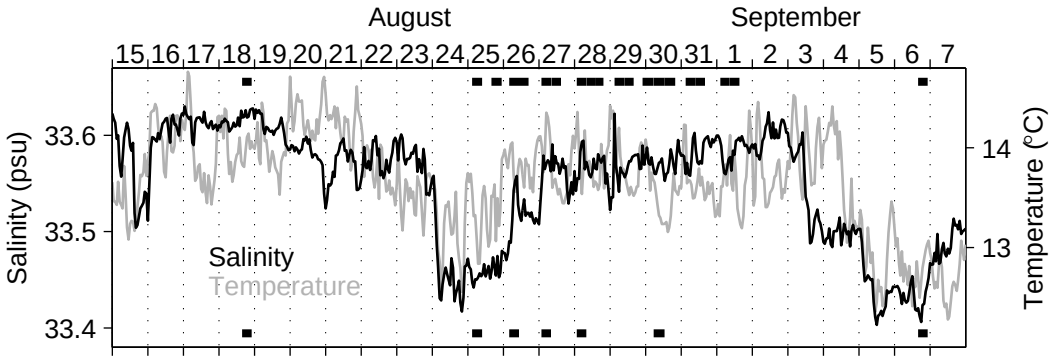
August
September
15 16 17 18 19 20 21 22 23 24 25 26 27 28 29 30 31 1 2 3 4 5 6 7
Salinity (psu)
33.6
33.5
33.4
Salinity
Temperature
14
13
Temperature (°C)

Figure 3

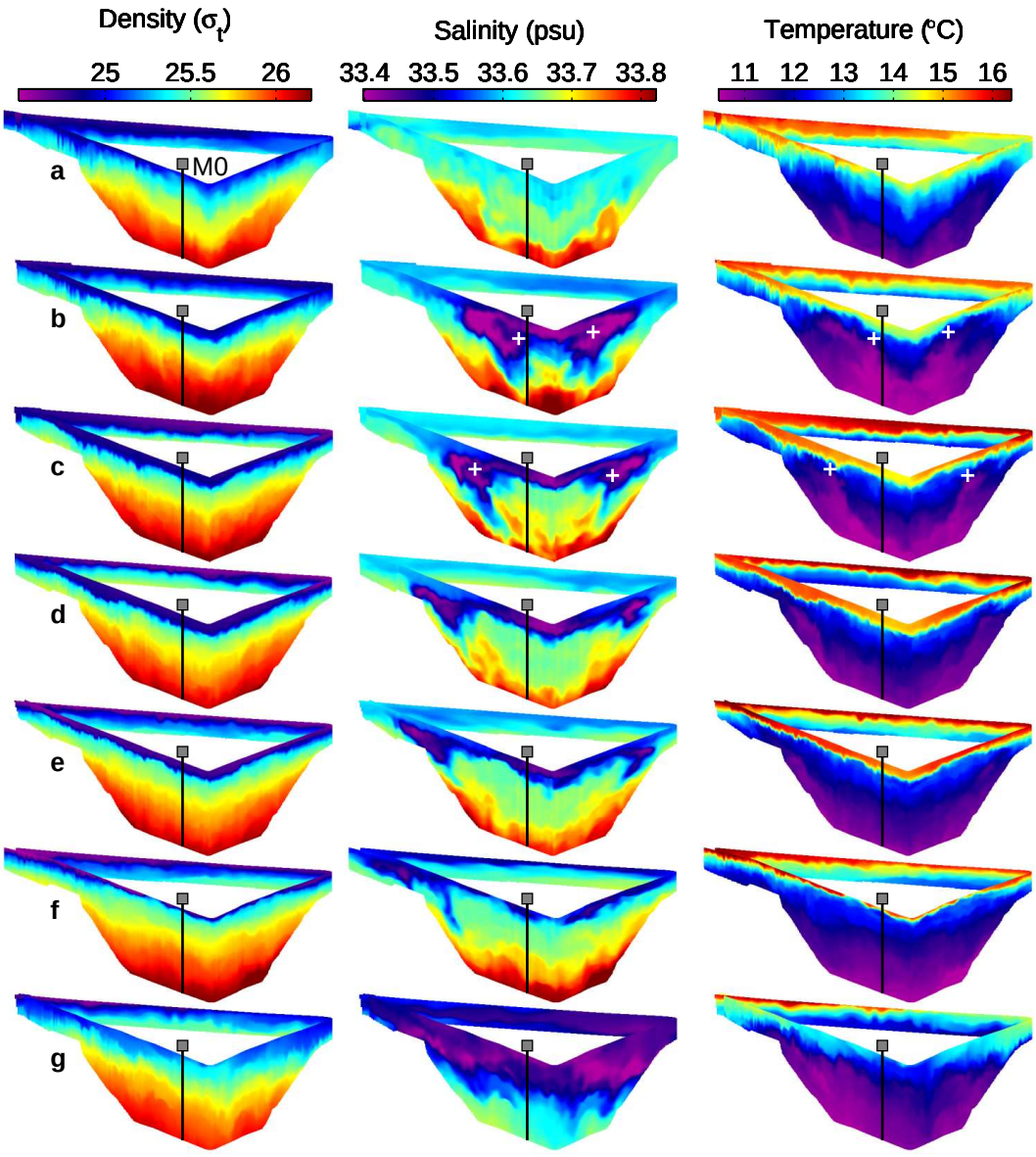
Density (σ_t)
25
25.5
26
Salinity (psu)
33.4
33.5
33.6
33.7
33.8
Temperature (°C)
11
12
13
14
15
16
a
M0
b
c
d
e
f
g

Figure 4

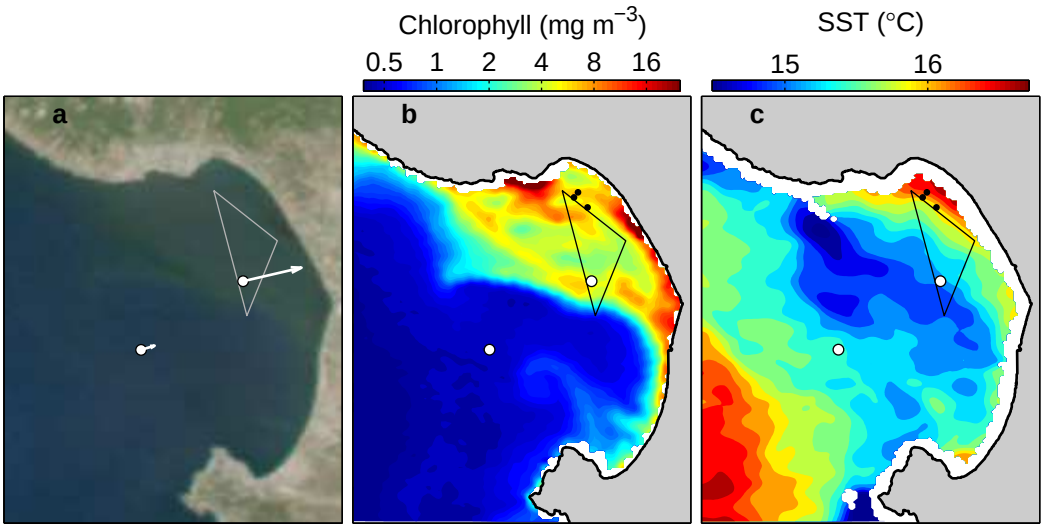

Figure 5

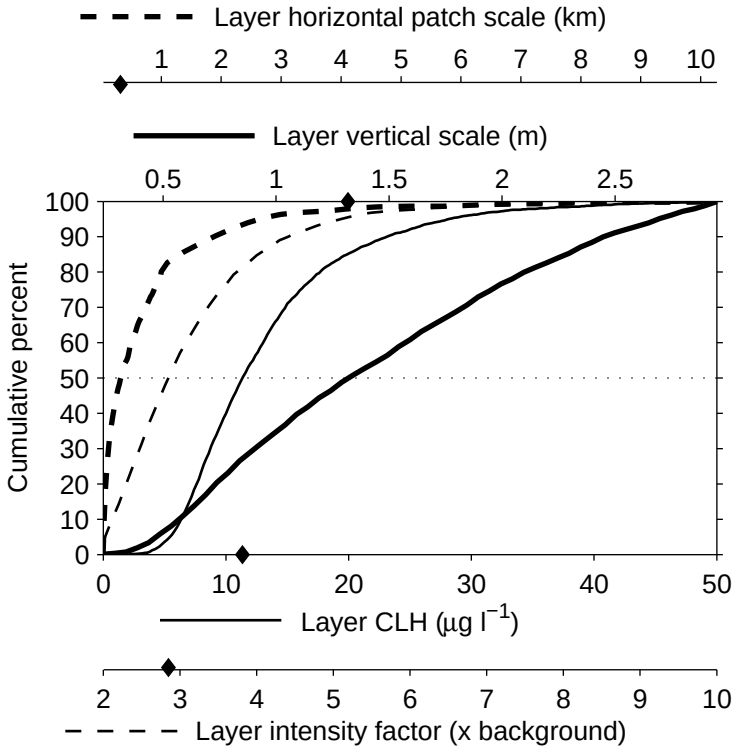
Layer horizontal patch scale (km)
1 2 3 4 5 6 7 8 9 10
Layer vertical scale (m)
0.5 1 1.5 2 2.5
Cumulative percent
100 90 80 70 60 50 40 30 20 10 0
0 10 20 30 40 50
Layer CLH (µg l−1)
2 3 4 5 6 7 8 9 10
Layer intensity factor (x background)

Figure 6

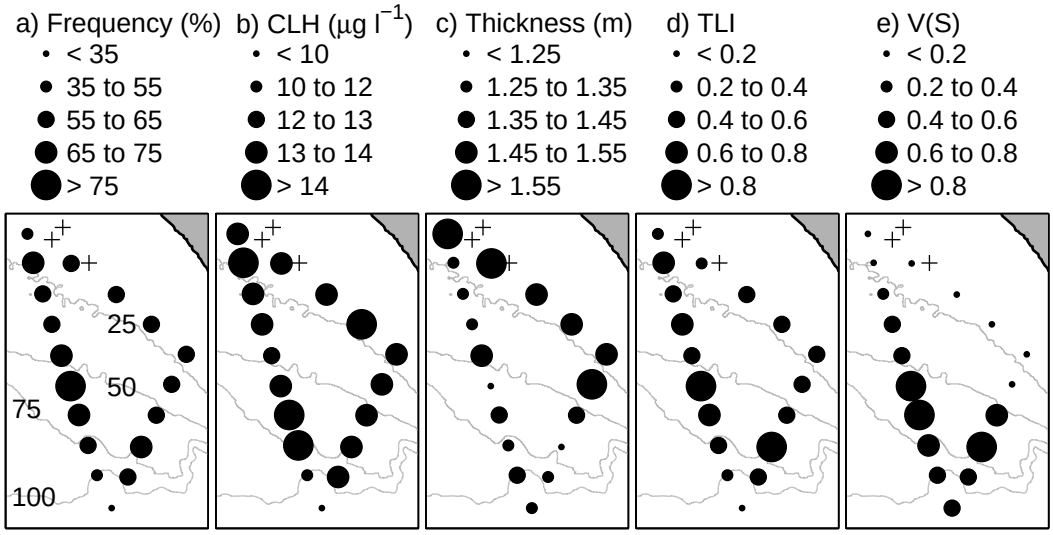
a) Frequency (%)
< 35
35 to 55
55 to 65
65 to 75
> 75
b) CLH (µg l^{-1})
< 10
10 to 12
12 to 13
13 to 14
> 14
c) Thickness (m)
< 1.25
1.25 to 1.35
1.35 to 1.45
1.45 to 1.55
> 1.55
d) TLI
< 0.2
0.2 to 0.4
0.4 to 0.6
0.6 to 0.8
> 0.8
e) V(S)
< 0.2
0.2 to 0.4
0.4 to 0.6
0.6 to 0.8
> 0.8
25
50
75
100

Figure 7

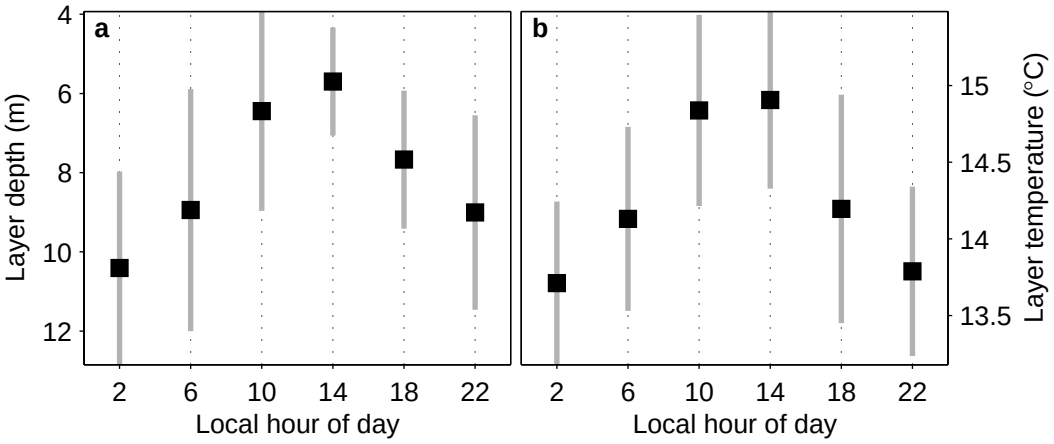
a
b
Layer depth (m)
4
6
8
10
12
2
6
10
14
18
22
Local hour of day
Layer temperature (°C)
15
14.5
14
13.5

Figure 8

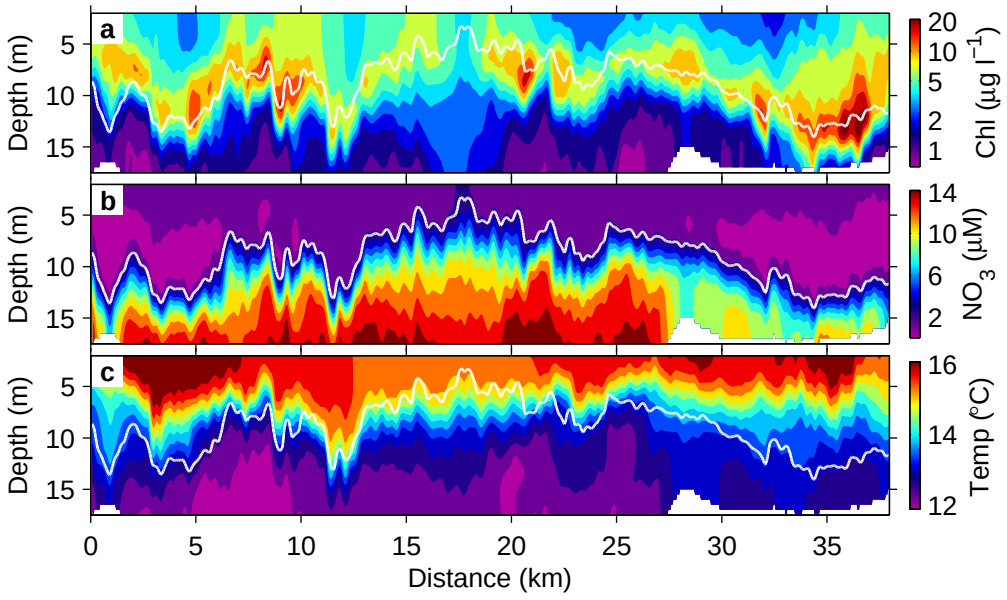
a
b
c
Depth (m)
5
10
15
0
5
10
15
20
25
30
35
Distance (km)
20
10
5
2
1
Chl (µg l^{-1})
14
10
6
2
NO$_3$ (µM)
16
14
12
Temp (°C)

Figure 9

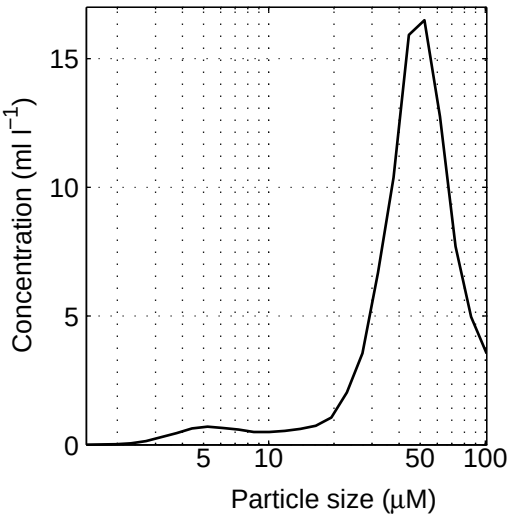

Figure 10

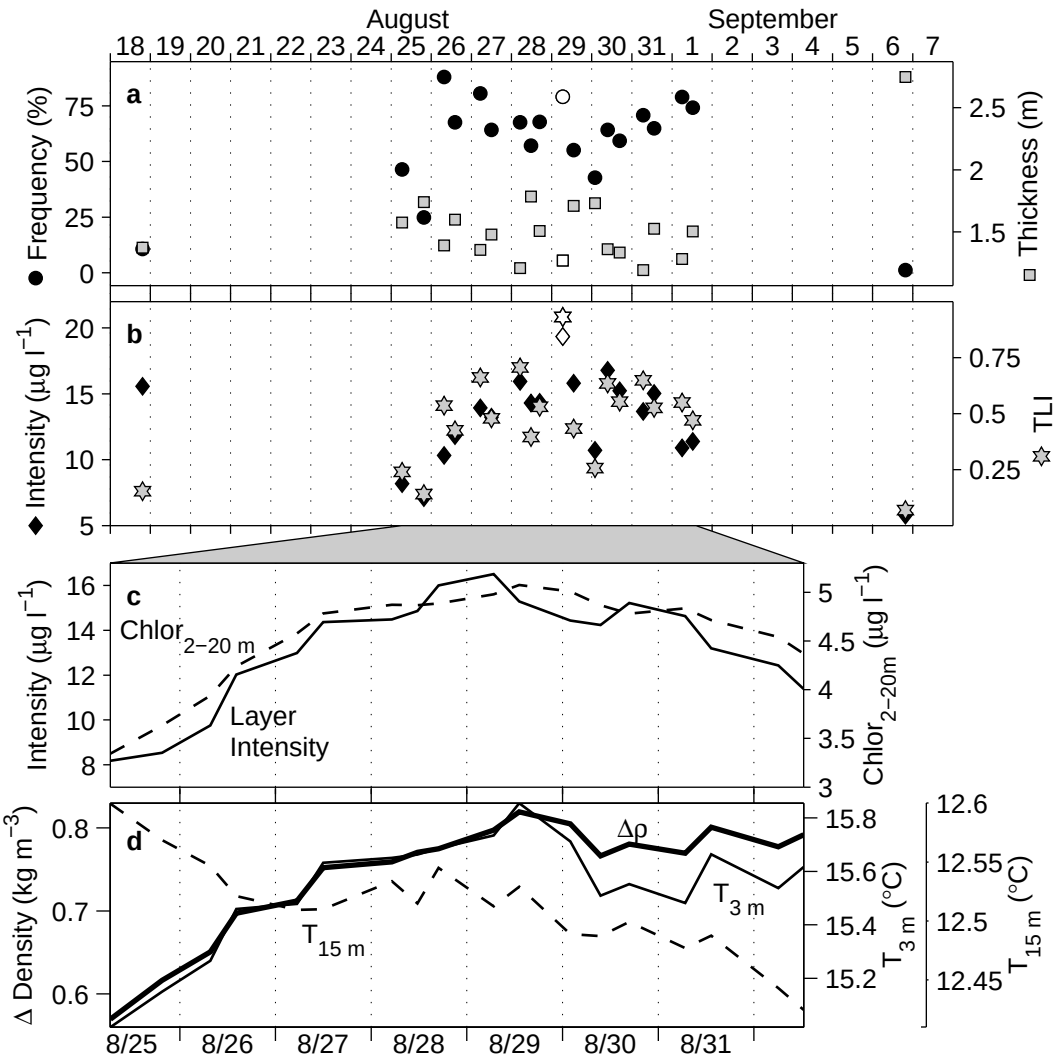
August
September
18 19 20 21 22 23 24 25 26 27 28 29 30 31 1 2 3 4 5 6 7
a
Frequency (%)
Thickness (m)
b
Intensity (µg l−1)
TLI
c
Chlor2−20 m
Layer Intensity
Intensity (µg l−1)
Chlor2−20m (µg l−1)
d
Δ Density (kg m−3)
Δρ
T15 m
T3 m
T3 m (°C)
T15 m (°C)
8/25 8/26 8/27 8/28 8/29 8/30 8/31

Figure 11

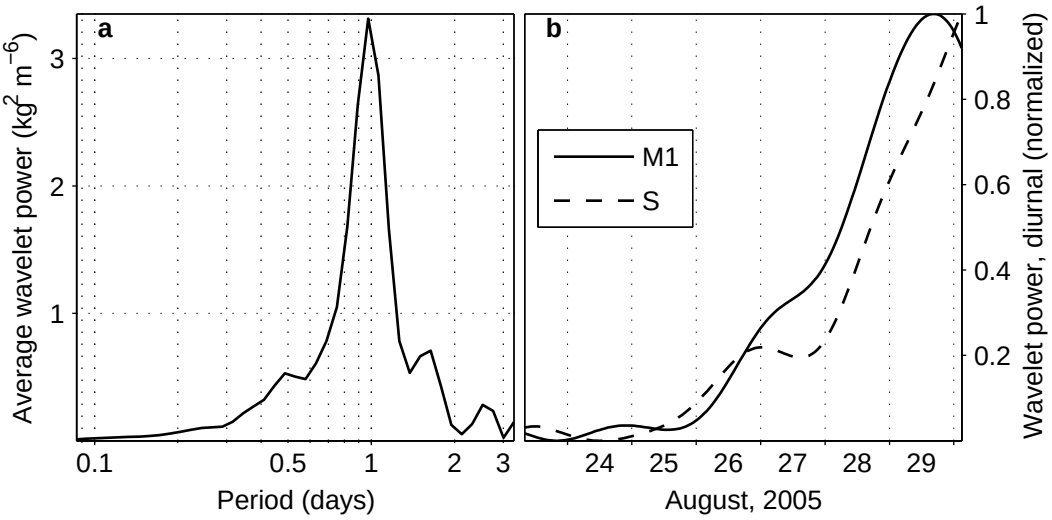
a
b
Average wavelet power (kg^2 m^{-6})
Period (days)
August, 2005
Wavelet power, diurnal (normalized)
M1
S
0.1
0.5
1
2
3
24
25
26
27
28
29
1
0.8
0.6
0.4
0.2

Figure 12

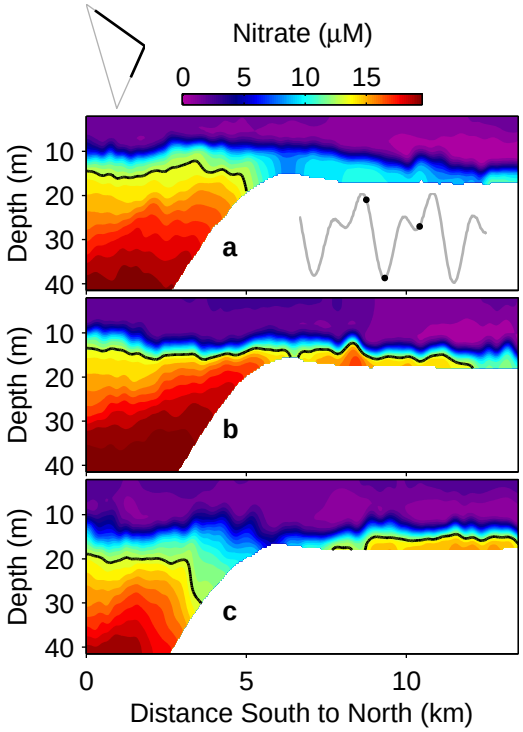
Nitrate (µM)
0
5
10
15
Depth (m)
10
20
30
40
a
b
c
0
5
10
Distance South to North (km)